Flicker Spectroscopy of Thermal Lipid Bilayer Domain Boundary Fluctuations

Cinzia Esposito,*† Aiwei Tian,* Svetlana Melamed,* Corinne Johnson,* Shang-You Tee,* and Tobias Baumgart*
*Department of Chemistry, University of Pennsylvania, Philadelphia, Pennsylvania, 19104; and †Dipartimento di Scienze Farmaceutiche, University of Salerno, 84084 Fisciano, Italy

ABSTRACT This contribution describes measurements of lipid bilayer domain line tension based on two-dimensional thermal undulations of membranes with liquid ordered/liquid disordered phase coexistence and near-critical composition at room temperature. Lateral inhomogeneity of lipid and protein composition is currently a subject of avid research aimed at determining both fundamental properties and biological relevance of membrane domains. Line tension at fluid lipid bilayer membrane domain boundaries controls the kinetics of domain growth and therefore regulates the size of compositional heterogeneities. High line tension promotes membrane domain budding and fission. Line tension could therefore be an important control parameter regulating functional aspects of biological membranes. Here the established method of fluid domain flicker spectroscopy is applied to examine thermal domain wall fluctuations of phase-separated bilayer membranes. We find a Gaussian probability distribution for the first few excited mode amplitudes, which permits an analysis by means of appropriately specialized capillary wave theory. Time autocorrelation functions are found to decay exponentially, and relaxation times are fitted by means of a hydrodynamic theory relating line tensions and excited mode relaxation kinetics. Line tensions below 1 pN are obtained, with these two approaches yielding similar results. We examine experimental artifacts that perturb the Fourier spectrum of domain traces and discuss ways to identify the number of modes that yield reliable line tension information.

INTRODUCTION

Since the original description of microscopically observable liquid ordered (Lo) and liquid disordered (Ld) phase coexistence in lipid bilayer membrane mixtures by Dietrich et al. (1) and by Samsonov et al. (2), long after the conception of the Lo membrane phase (3), the understanding of the underlying physical chemistry of fluid bilayer phase coexistence has considerably progressed, as summarized in a recent review by Veatch and Keller (4). Temperature and composition dependence of lipid-mixing/demixing transitions have been investigated extensively (5–9). The composition and phase-partitioning dependence of lipid fluorophore diffusion (10,11) as well as fluid domain diffusion (12) have been analyzed. Three-dimensional membrane shapes modulated by differing elastic properties of coexisting liquid phases have been described (6,13,14), and quantitative analysis of these shapes has confirmed aspects of elastic membrane theories (13,15). Although these phenomena present interesting soft condensed matter physics problems, research in this area is especially driven by the vivid discussion surrounding functionally important lipid/protein membrane heterogeneities in living cells (16,17).

An aspect of lipid bilayer membrane phase coexistence that is receiving increasing attention, both from theory (18–21) and experiments (13,15,22–25), are properties of domain boundaries, notably the interfacial tension (line tension) associated with coexisting domains. Generally, the concept of line tension was introduced by Gibbs in his theory of capillarity (26). Most experimental and theoretical studies of line tension to date have examined three-phase contact systems (27). Line tension is also found in surface phase contact regions, where it is termed ''boundary tension'' (28). However, unlike the line tension in three-phase contact systems, the one occurring at surface phase contacts has been studied experimentally in a few material layers only, including Langmuir layers of polymers (29,30) and surfactants (31), as well as lipids.

Line tension at lipid monolayer gas and liquid-expanded phase domain boundaries was measured by Knobler's group (32). McConnell and co-workers determined line tensions at fluid/fluid phase boundaries in a cholesterol (Chol)/dimyristoylphosphatidylcholine monolayer by measuring the recovery rate of distorted domain shapes to equilibrium (33) and found values that varied between 0.1 and ~10 pN, dependent on the film pressure. As expected, line tension decreased toward the critical point of phase coexistence for this system. The shape-distorting shear flows used in that study (33) were replaced by deformation forces applied by laser tweezers (34) to yield line tensions at liquid-expanded/gas phase boundaries of a surfactant monolayer. Analysis of thermally induced domain shape fluctuations gave line tensions at lipid monolayer fluid domain boundaries ~0.1 pN near the critical point (35). Theoretical examination of domain line tension in lipid monolayers has been based on both continuum (33,35) and microscopic models (18,19,36), the latter giving values ~1–10 pN.

Lipid bilayer line tensions arise both at a membrane edge (vesicle pore) and at the domain boundary of phase-separated but otherwise continuous membranes. Bilayer membrane edge

Submitted May 2, 2007, and accepted for publication June 28, 2007.

Address reprint requests to Tobias Baumgart, Tel.: 215-573-7539; E-mail: baumgart@sas.upenn.edu.

Editor: Thomas J. McIntosh.

0006-3495/07/11/3169/13 $2.00

doi: 10.1529/biophysj.107.111922

tensions were determined both experimentally (37–39) and theoretically (40), with values near ~10 pN. Shape analysis of giant unilamellar vesicles (GUVs) yielded rough phase boundary line tension estimates for fluid/fluid phase coexistence in the range of ~1 pN (13,15). Line tensions of domains in membranes with fluid/solid phase coexistence have been determined by analyzing nucleation rates measured by atomic force microscopy (25). We have recently measured line tensions of values up to ~5 pN via micropipette aspiration of dumbbell-shaped vesicles with fluid/fluid phase coexistence (22). This method gives access to large line tensions but becomes increasingly inaccurate below line tensions of ~0.5 pN. Near mixing/demixing transition temperatures, thermal in-plane undulations of bilayer domains around a circular average shape can be observed (13) and spectrally analyzed by Fourier decomposition. The mean-squared powers of undulation modes can be related to line tension by capillary wave theory (13,35,41). Our research follows qualitative observations (13) and is further motivated by recent measurements from the Keller lab, where temperature-dependent power spectra of bilayer domain fluctuations were reported and analyzed to yield line tensions (23) by an approach described by Safran (see (56)), which is similar but not equivalent to the one detailed below, which is based on Goldstein and Jackson (35).

This contribution is organized as follows. In the next section we introduce general aspects of surface fluctuations and review capillary wave theory (35) specialized to a situation where fluid domain boundaries in the size range of a few micrometers, as examined by optical microscopy, fluctuate with constrained domain area. This constraint, in conjunction with the assumption that the Fourier transformed phase boundary is representable by a set of independent harmonic oscillators, predicts spectral powers of undulation modes proportional to $1/(n^2-1)$ (35), where n is the mode number, as observed in fluctuating monolayer domains (35,41), and experimentally confirmed below for bilayer domains. A Materials and Methods section follows where experimental details are provided and shape tracing and analysis are outlined. The Results section first demonstrates that the amplitudes of mode fluctuations follow a Gaussian probability distribution, which is a requirement for the applicability of standard capillary wave theory and also results in thermal energy equipartitioning among normal modes.

We then proceed to show how the experimentally limited number of modes that analytically behave according to equipartitioning harmonic oscillators can be identified to yield reliable line tension values and be distinguished from mode powers significantly distorted due to optical resolution limit, image pixelization, random noise, and finite fluorescence camera integration time. We obtain line tensions from mean power analysis of fluctuation profiles of micrometer-sized domains in GUVs with mixed lipid membranes. Furthermore, time autocorrelation of the static squared Fourier coefficients yields mode relaxation times that, via a hydrodynamic theory by Stone and McConnell (42), are related to line tension and aqueous fluid viscosity. Relaxation times are shown with increasing mode number to quickly approach fluorescence camera frame acquisition time. We find that line tensions strongly depend on illumination time, as has previously been observed (43). The method of domain flicker spectroscopy can yield reliable line tension estimates in a regime not accessible by complementary methods (13,22).

Undulation spectroscopy and capillary wave theory

Thermally excited surface undulations of fluid-like objects with closed boundaries have been examined theoretically and experimentally and include fluctuations of fluid drops and spherical emulsions (44–46), as well as normal (out-of-plane) undulations of lipid bilayer membranes in GUVs and red blood cells (47–50) and in-plane fluctuations of domain boundaries in Langmuir films of lipids (41) and polymers (51). Flicker spectroscopy via microscopy imaging and spectral analysis of thermally fluctuating vesicles has matured into a well-established technique to measure membrane-bending stiffness, with increasing levels of accuracy (52–54). When evaluating the bending stiffness of GUVs from shape fluctuations, fluctuation modes with lowest mode numbers typically have to be discarded (52,54). Conversely, in domains with diameters of just a few micrometers with in-plane fluctuations, only the first few mode numbers contain reliable line tension information.

Classical capillary wave theory

The equation that we require to relate spectral coefficients, $\langle|u_n|^2\rangle$ to line tension is based on capillary wave theory appropriately specialized to our experimental situation (35). In the following, we discuss essential components of the underlying theory. Capillary wave theory assumes that fluctuations of a system containing an interface can be derived from an effective Hamiltonian (55,56) that, for our experimental system, is written $H=\sigma L=\sigma\int_0^{2\pi}\sqrt{r^2+(\partial r/\partial\theta)^2}d\theta$, where σ is the line tension, L is the domain boundary contour length, r is the distance of the contour from the center of mass of the fluctuating domain, and θ is the polar angle. This Hamiltonian is difficult to treat analytically and is therefore expanded and truncated to yield $H=\sigma\int_0^{2\pi}(r+(1/2r)(\partial r/\partial\theta)^2)d\theta$. This approximation is valid for small deviations of r from the value of R_0 defined below. The contour coordinates are expanded in a Fourier series according to (see the appendix for details) $r(\theta)=R_0(1+u_0+\sum_{n=1}^{N/2}a_n\cos n\theta+\sum_{n=1}^{N/2}b_n\sin n\theta)=R_0(1+u_0+(1/2)\sum_{n\neq0}u_n\exp(in\theta))$, where the summation index n on the right-hand side is a number between $-N/2$ and $N/2$, $N=L/b$, L is the contour length, and b is a cutoff length of molecular dimension (56). The contour length and domain area A can be expressed as (see appendix)

$$L=2\pi R_0\left[1+u_0+\frac{1}{4}\sum_n n^2|u_n|^2\right] \quad (1)$$

$$A = \pi R_0^2 \left[(1 + u_0)^2 + \frac{1}{2} \sum_n |u_n|^2 \right]. \quad (2)$$

We are interested in examining fluctuations of domain boundary profiles of a membrane domain with fixed domain area $A = \pi R_0^2$, where R_0 is the equivalent radius of a non-fluctuating domain. This expression yields with Eq. 2 the relation $(1+u_0)^2 = 1 - (1/2)\sum_n |u_n|^2$, which allows eliminating u_0 from Eq. 1 with the expansion $1+u_0 \approx 1 - (1/4)\sum_n |u_n|^2$ to yield for the contour length $L = 2\pi R_0(1+(1/4)\sum_n (n^2-1)|u_n|^2)$. Hence we obtain for the thermal energy ΔE of the fluctuating boundary $\Delta E = (\sigma\pi R_0/2)\sum_n (n^2-1)|u_n|^2$, equivalent to an expression derived in Goldstein and Jackson (35). Note that the mode amplitudes $|u_n|$ are dimensionless, as opposed to the definition given by Goldstein and Jackson (35). With approximations inherent in this approach, the thermal motion of the contour can be described by a set of independent harmonic oscillators, where the probability to find a certain vibrational amplitude $|u_n|$ in a single snapshot of the domain is Gaussian (56): $P_n(|u_n|) \propto \exp(-(\sigma\pi R_0(n^2-1)|u_n|^2/2kT))$. The (dimensionless) variance of this Gaussian is given by

$$\langle |u_n|^2 \rangle = \frac{kT}{\sigma\pi R_0 (n^2-1)}. \quad (3)$$

Eq. 3 also follows from thermal energy equipartitioning (13,35), which implicitly assumes oscillators with quadratic degrees of freedom. Only after experimentally demonstrating that this assumption holds, as we do below by explicitly determining fluctuation probability distributions, can Eq. 3 be used to measure line tension σ associated with normal modes with index n. From Eq. 3, mean values of real space fluctuations are obtained by summing over n to yield (21,56)

$$\langle \Delta r(\theta)^2 \rangle = \frac{3kTR_0}{4\sigma\pi}.$$

MATERIALS AND METHODS

Lipids dioleoylphosphatidylcholine (DOPC), dipalmitoylphosphatidylcholine (DPPC), and Chol were obtained from Avanti Polar Lipids (Alabaster, AL) and used without further purification. Lipid stock solutions were prepared in chloroform, and phospholipid solution concentrations were quantified on a weekly basis by a standard colorimetric phosphate assay. Vesicles were fluorescence labeled by addition of 0.2 mol % of the lipid fluorophore Texas Red dihexadecanoylphosphatidylethanolamine (Invitrogen, Carlsbad, CA). GUVs were prepared by the standard method of electroswelling (57) in 100 mM sucrose solution using indium tin oxide covered glass (Delta-Technologies, Stillwater, MN), exerting an electrical field of 2 V/mm at frequency 5 Hz for 2 h at 60°C. Note that a recent report provided an alternative electroswelling method, reducing lipid oxidation that can influence line tensions (43). Flicker spectroscopy will allow, in future experiments, the comparison of line tensions measured in vesicles obtained from these two different swelling methods. Vesicles were allowed to cool to room temperature for 1 h and imaged immediately in a chamber consisting of a microscope slide and coverslip separated by a silicon grease rectangle that enclosed a vesicle dispersion of volume 5 μl.

Imaging

Fluorescence time sequences of fluctuating vesicles were obtained with an inverted microscope (IX81; Olympus, Center Valley, PA), with a 60× 1.2 numerical aperture water immersion objective with coverslip correction (Olympus), a Texas Red filter cube (Chroma, Rockingham, VT), and a back-illuminated electron microscopy-charge-coupled device (EM-CCD) camera (ImagEM; Hamamatsu, Bridgewater, NJ). The pixel size is fixed by our optical setup at 1/3.78 μm, close to the point spread function (PSF) width of the optical microscope. This pixel size is larger by a factor of 2–3 than the optimum value given by the Nyquist theorem but allowed us to minimize frame acquisition times to more accurately determine mode dynamics. The same setup could be used for confocal microscopy imaging by means of a FLUOVIEW-300 scanhead (Olympus). All vesicles were prepared with a composition referring to DOPC/Chol/DPPC molar ratios of 1:1:1, which is a composition where both homogenous and phase-separated vesicles are found at room temperature (21°C ± 1°C).

This observation indicates that this composition is close to a mixing/demixing phase boundary (58), which is further demonstrated by the fact that all vesicles phase separated at room temperature upon illumination (6,43,59) with excitation light (from an HBO 100 mercury burner; Olympus) passed through a band-pass filter (D540/25×, Chroma). Vesicles that were observed to be phase separated in the absence of a light-dependent induction period showed domain boundary fluctuations of domains typically too large to be analyzable by flicker spectroscopy (see below). We used the effect of photoinduced phase separation to obtain domains no larger than ~20% of the vesicle radius. After a coarsening period of several minutes, the radii of these domains were stable over the time course of our experiments (less than 5 min). Immediately after the first optically noticeable occurrence of membrane heterogeneity, the light intensity was reduced by means of optical density (OD) filters with OD values as indicated in the experimental section. We note that we could induce an equivalent demixing transition by lowering the temperature, typically by 2°C–3°C at minimized excitation light intensity.

Simulation of domain shapes

Synthetic domain contours were obtained from a set of 10 randomly generated Fourier coefficients, a_n and b_n, respectively. These were generated from random numbers obeying a Gaussian distribution (60), weighted by Eq. 3, and then uniformly scaled to yield a microcanonical contour ensemble. Synthetic ''experimental'' images were obtained by first generating a pixel trace of intensity value I_d in an image of pixel dimension 10 times larger than the final image, setting intensities of pixels contained within the trace boundary to I_d, convolving the obtained domain shape with a two-dimensional Gaussian with a variance corresponding to the optical PSF (relative to the domain radius) and then reducing the pixel dimension of the image by a factor of 10. Additionally, Poisson noise was added to the domain image by replacing the undistorted pixel intensity by random numbers drawn from a Poisson distribution with a variance equivalent to the original pixel intensity.

Shape tracing and raw data processing

Image processing and data analysis were performed with the software MATLAB (The Mathworks, Natick, MA). Our initial data analysis followed procedures similar to those described by Seul et al. (61). Gray scale image series were initially converted frame by frame into binary images using automated thresholding, allowing localization of the domain ''centers of mass''. Pixel intensities in an area surrounding the domain center I_{in}, as well as in an area element of equal size outside the domain I_{out}, were measured in the original image to define a new global threshold with value $(I_{in} - I_{out})/2$ used to obtain a second binary image suitable for tracing domain boundaries. Potentially, the spatial resolution of this approach can be further improved by gray level profile fitting (54,62). The parameter $R_0 = (A/\pi)^{1/2}$ was obtained from the domain area A. Shape sequences where the radius R_0

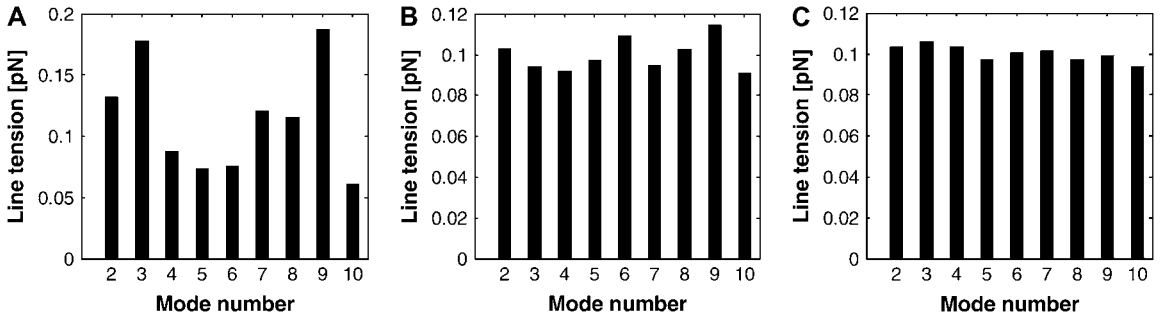

FIGURE 1 Distributions of apparent line tension values obtained from FFT analysis of simulated sets of fluctuating domain coordinates with nominal line tension 0.1 pN (see Materials and Methods section for details) of 10, 100, and 1000 frames (from *left* to *right*), illustrating the dependence of mean mode power fluctuations according to $1/\sqrt{M}$, where M is the number of analyzed boundary traces.

changed by amounts above the tracing noise level (for example, by merger of two adjacent domains) were discarded. Shape trace coordinates $[y(x), x]$ were converted into polar coordinates $[r(\theta), \theta]$ and the shape deviations $\Delta r(\theta) = r(\theta) - \langle r(\theta)\rangle$ from the average value $\langle r(\theta)\rangle$ were spectrally analyzed via fast Fourier transform (FFT). Note that $\langle r(\theta)\rangle = R_0(1 - (1/4)\sum_n \langle|u_n|^2\rangle)$ (see appendix) and therefore $R_0 \neq \langle r(\theta)\rangle$ for fluctuating domains. FFT of $\Delta r(\theta)$ yields spectral powers $|u_n(t_i)|^2$ for every trace with index i at time t_i, from which time-averaged mean powers $\langle|u_n|^2\rangle$ were obtained and assumed to equal ensemble averages.

Obviously, to estimate mean powers with sufficient confidence levels, a sufficient number of frames must be averaged. Fig. 1 shows tracing results of simulated frames of fluctuating domains to demonstrate how the variance of line tensions obtained from different modes decreases with increasing number of averaged frames. We chose to average a number of $M = 500$ frames for each line tension measurement. Alternatively, to obtaining $|u_n|^2$ values from FFT analysis of $\Delta r(\theta)$, the angular autocorrelation function $c(\delta) = \langle\Delta r(0)\times\Delta r(\delta)\rangle$ was determined, where δ is a phase shift. Analytically, the angular autocorrelation function is related to the trace Fourier mode amplitudes according to $c(\delta) = (R_0^2/2)\sum_n |u_n|^2\cos(n\delta)$. Therefore, $\langle|u_n|^2\rangle$ follows from Fourier transform of $c(\delta)$ and averaging the values for individual traces. Additionally, the time autocorrelation functions $g_n(\tau) = \langle\Delta|u_n(\tau)|^2\times\Delta|u_n(0)|^2\rangle$ were obtained by time autocorrelating spectral powers for each mode number n. Here, $\Delta|u_n(t)|^2 = |u_n(t)|^2 - \langle|u_n(t)|^2\rangle$. The functions $g_n(\tau)$ are expected to decay exponentially (44,63), which is experimentally confirmed below. We therefore fitted $g_n(\tau)$ with a single exponential to yield mode relaxation times τ_n.

RESULTS

GUVs with composition of DOPC/Chol/DPPC = 1:1:1 were prepared by electroswelling at 60°C, cooled to room temperature, and then imaged immediately. Preparations of GUVs typically show a large range of different vesicle diameters (57) with average values that vary between preparations. To not bias results, we focused on medium-sized vesicles with diameters in the range of 25–37 μm. For domain flicker spectroscopy, domains were chosen with radii ~20% of the vesicle radius to minimize distortion of the image of the fluctuating domain profile through deviation from a planar membrane. Domain fluctuations were analyzed only if the center of mass of the domain remained close to the vesicle pole during the timescale of the image acquisition. Deviation from planar membrane profiles can furthermore result from thermal three-dimensional vesicle shape fluctuations (47–50). Since these out-of-plane membrane undulations contribute to phase boundary fluctuations, we focused on vesicles that were sufficiently swollen that undulations normal to the membrane were sufficiently suppressed. Accordingly, after each image sequence of a fluctuating domain was determined, every vesicle was examined for its three-dimensional shape by obtaining a confocal z-scan, and both visibly undulating vesicles and those deviating from a spherical shape were discarded.

Fig. 2 shows random snapshots of a fluctuating domain on the north pole of a GUV, i.e., on the vesicle surface farthest away from the inverted microscope's objective. The domain shows a radius of 3.4 μm in a vesicle of 37 μm diameter. Domains were imaged using a 10 ms exposure time per

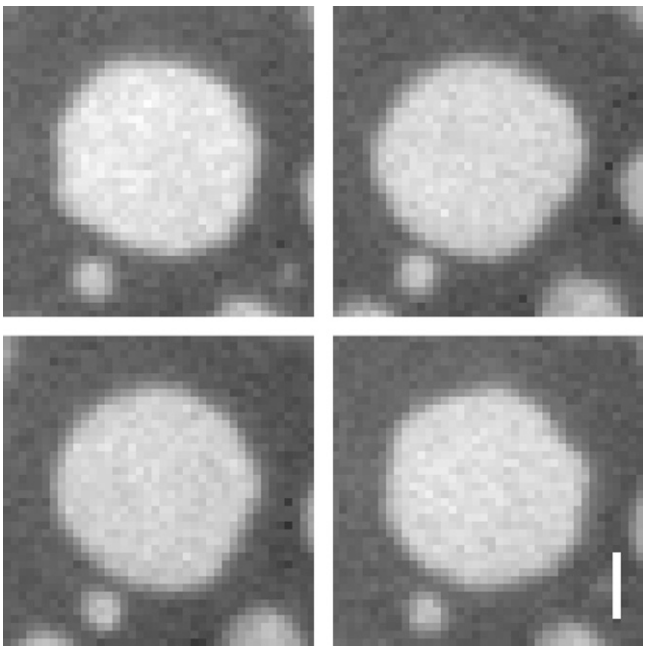

FIGURE 2 Random CCD camera snapshots of a fluctuating Ld phase domain on the north pole of a GUV, i.e., farthest away from the microscope objective. The vesicle diameter is 37 μm, and the domain radius amounts to ~3.4 μm. Bar: 2.5 μm.

frame and frame capture rate of 90 frames per second. Fig. 3 illustrates single frame analysis results for the upper left domain shown in Fig. 2. Comparison of the domain trace in Fig. 3 *A* with the domain in Fig. 2 *A* indicates that boundary tracing of binary images obtained through thresholding discards some trace information. Boundary tracing by grayscale gradient analysis may allow subpixel size resolution boundary tracing and could be implemented in future work. In Fig. 3 *B*, the domain radius is plotted in pixel dimension versus the polar angle. The plot reveals boundary localization noise stemming from image pixelization. The Fourier transform of the same trace, which is depicted in Fig. 3 *C*, indicates that the second and fourth mode dominate this particular shape, which is also revealed in the angular autocorrelation function of the trace (Fig. 3 *D*). Analysis of numerous traces allows us to determine mode power statistics that can reveal both fluctuation mechanism and magnitude of the boundary elongation restoring force: the line tension. Previous studies have averaged spectral information from 10–20 frames (41). However, as the tracing results of simulated fluctuating domains in Fig. 1 show, a large number of frames must be analyzed to yield average mode amplitude values with sufficient certainty.

We found that the probability distribution of mode powers obtained from analysis of 500 consecutive frames is well fitted by an exponential decay; the distributions for the first four modes (mode numbers 2–5) of a fluctuating domain with radius $\sim$3 μm and vesicle radius 28 μm are shown in Fig. 4. This observation indicates that mode amplitudes follow a Gaussian probability distribution, which is a necessary requirement for employing the equipartition theorem to relate mean values of mode powers to line tension. According to Eq. 3, the variance of the Gaussian probability distribution, experimentally obtained from the exponential decay constants in Fig. 4, *A–D*, should be a linear function of the mode factor $1/(n^2 - 1)$. This linear relation is confirmed in Fig. 4 *E* for the first four modes. As we demonstrate below, a limited number of modes, depending on experimental conditions, is observed to follow this linear relationship. From the slope in Fig. 4 *E*, a line tension of 0.12 pN is obtained. We furthermore ensured that every analyzed domain showed constant domain area over the time course of the experiment, as demonstrated by the value of the equivalent radius R_0, which is obtained from the domain area. Measurements where R_0 yielded systematically nonconstant values, caused, for example, by domain fusion or out-of-focus movement of the domain, were discarded.

We determined probability distributions of mode powers for all domains that were analyzed and found them to be uniquely exponential. This observation justifies calculating mean mode powers to obtain line tensions. Mean values of spectral densities shown in Fig. 4 were determined by direct FFT of the boundary trace. It has previously been shown that an alternative approach, via computation of angular autocorrelation functions (Fig. 3 *D*) followed by Fourier transform, suppresses noise contributions to spectral densities (52,64). Our analysis software routinely computes these alternatively obtained mode powers; however, we have not found this approach to be advantageous compared to direct Fourier transform of the boundary trace and therefore follow this latter method. Fig. 5 *A* plots the mean values of mode powers up to the mode $n = 11$. This representation, however,

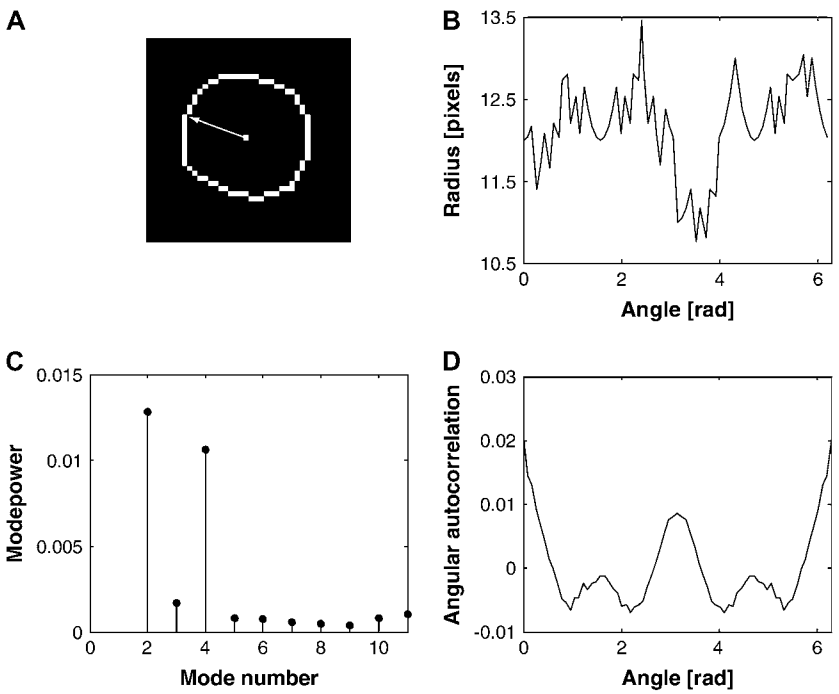

FIGURE 3 All figures are related to the domain in Fig. 2 *A*. (*A*) Domain boundary trace with center of mass indicated by the middle pixel. (*B*) Domain radius in pixel units as a function of polar angle. The angle is measured clockwise from the pixel indicated with an arrow in *A*. Pixelization noise is observed. (*C*) Fourier transform of the trace, indicating second and fourth mode to dominate this particular trace snapshot. (*D*) Angular autocorrelation function, which can be Fourier transformed to determine mode powers, as in *C*. Mode powers are equivalent to $R_0^2|u_n|^2$ in units of μm^2.

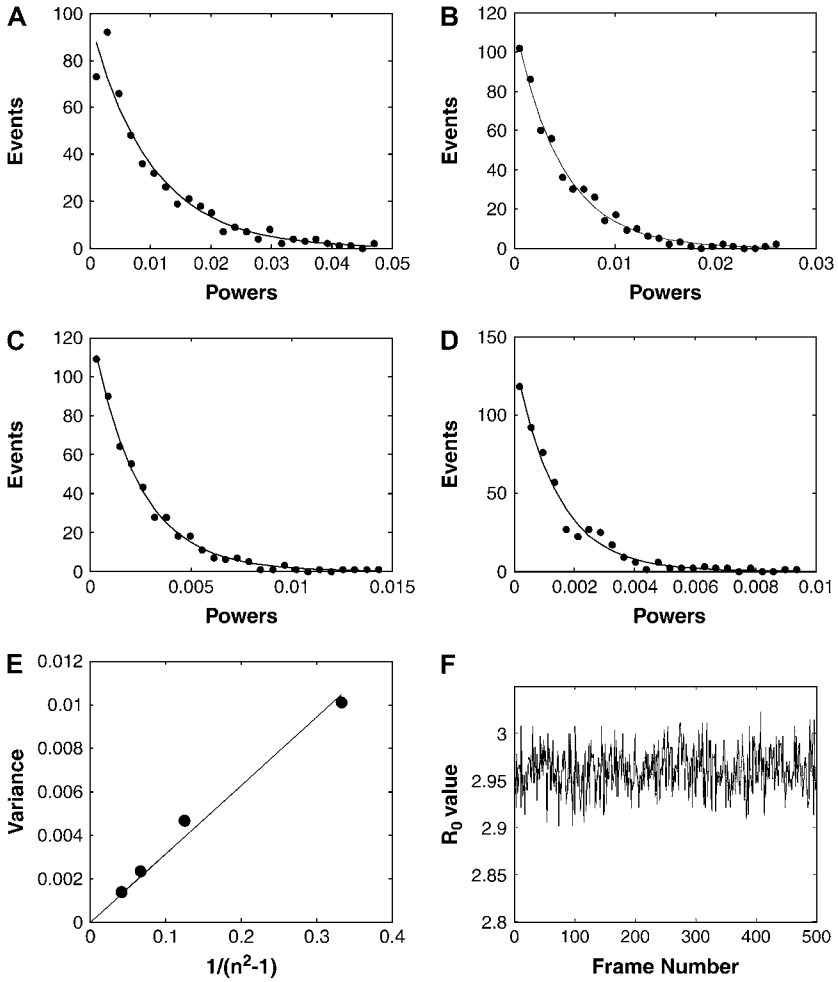

FIGURE 4 (*A–D*) Fourier mode power probability distribution analysis obtained from an image sequence of a fluctuating domain with a radius of ~3 μm, in a spherical vesicle of diameter 28 μm. Mode powers $|u_n|^2$ are obtained from direct Fourier transform of angular domain traces and are plotted as $R_0^2|u_n|^2$ in units of μm^2. Probability distributions for mode powers 2–5 (from *A* to *D*) are well fit by an exponential decay, indicating an underlying Gaussian distribution of mode amplitudes $|u_n|$. The decay constants of the exponential functions yield the variances of Gaussian mode amplitude distributions. (*E*) The slope of the plot of the distribution width (variance) versus the mode index factor is related to line tension (see Eq. 3): in this experiment a value of 0.12 pN is obtained. (*F*) The value R_0, which is the equivalent radius of a nonfluctuating domain, indicates that the domain area remains constant (within noise levels) during our experiment.

does not easily reveal which modes are analyzable by means of capillary wave theory. As in Fig. 1, we therefore plot apparent line tensions obtained from mean mode powers shown in Fig. 5 *A* by means of Eq. 3 against mode number (Fig. 5 *B*). This representation reveals that only modes 2–5 follow the capillary wave model Eq. 3, since higher modes are observed to progressively deviate from the average line tension of low number modes indicated by the dashed line in Fig. 5 *B*. The line tension values inferred from modes 2–5 are in agreement with the value determined from the plot shown in Fig. 4 *E*.

Note that an analysis that neglects finite system size, which instead of Eq. 3 would lead to $\langle|u_n|^2\rangle = (kT/\sigma\pi R_0 n^2)$, equivalent to the more familiar expression $\langle|u_n|^2\rangle \propto (kT/\sigma q^2)$, where q is the wave vector (56), would further truncate the range of analyzable modes toward lower mode numbers. Although such a simplified approach is being used in systems where many fluctuating modes are accessible (54), in small domains of phase-separated vesicles only the first few modes are microscopically resolvable, and finite system size should be considered. This fact is further demonstrated via a graph that was introduced in Goldstein and Jackson (35), shown in Fig. 5 *C* where we plot the second mode mean power/higher mode mean powers ratio, $\langle|u_2|^2\rangle/\langle|u_n|^2\rangle$. According to Eq. 3, such a plot should show a slope of 1/3, which is observed for the first four modes in Fig. 5 *C*. Note that in lipid monolayer domains, contrary to bilayers, dipolar long-range interaction leads to an upward deviation from the 1/3 slope straight line shown in Fig. 5 *C* (35). In our case, this suggests absence of measurable long-range dipolar interactions in our bilayer system.

Until now, we have examined the statistics of static domain boundary profiles. However, time lapse recording of domain traces can also reveal dynamic information about our system of independent oscillators. We therefore compute time autocorrelation functions for the first four Fourier modes (2–5) as shown in Fig. 6, *A–D*. As expected (44,63), the experimental autocorrelation functions are well fit by exponentials, and the decay constants yield the relaxation times τ_n of excited modes with index n. Correlation times are observed to decrease with increasing mode index. Similar observations have been made in lipid monolayer films (65). Hydrodynamic theories can be devised that relate thermal fluctuation mode relaxation times to line tensions (42,51,66).

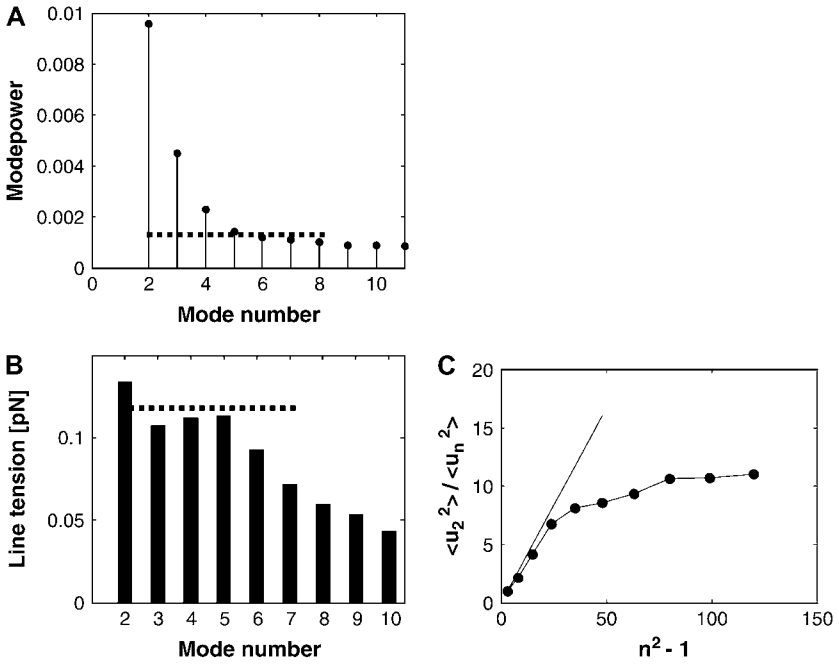

FIGURE 5 Fourier mode mean power analysis of the same fluctuating domain as examined in Fig. 4 *A* shows the mean mode powers $R_0^2\langle|u_n|^2\rangle$ in units of μm^2 as a function of mode number, obtained from the analysis of 500 image frames. Apparent line tension values in *B* indicate that a limited number of modes can be examined accurately for mode line tensions. In *A* and *B*, the dashed line indicates the range of modes amenable to capillary wave theory analysis (ideally all modes will show similar line tensions, see Fig. 1 *C*). (*C*) Plot of the second mode mean power divided by higher mode mean powers against the factor $n^2 - 1$. This plot is expected to be linear, with slope 1/3 (indicated by the *straight line*) for a domain with constrained area amenable to capillary wave analysis (see main text).

According to an approach due to Stone and McConnell (42) (see also Mann et al. (51) and Alexander et al. (66)), domain relaxation times in lipid films supported by an aqueous subphase are given by an expression equivalent to

$$\tau_n = \frac{2\pi r^2 \eta}{\sigma} \frac{(n^2 - 1/4)}{n^2(n^2 - 1)}, \quad (4)$$

where η is the viscosity of the subphase. Accordingly, this approach assumes domain dynamics to be dominated by the viscosity of the aqueous membrane surroundings and neglects the viscosity of the membrane itself (67). Eq. 4 has been modified from the form suitable for subphase-supported monolayers (42,51,66) by introducing a factor of 2 to account for the presence of two deep aqueous layers surrounding the bilayer membrane. Eq. 4 predicts a linear relationship between the *n*-dependent mode factor and the mode correlation times. This relationship is confirmed in Fig. 6 *E* for the first four modes of the fluctuating domain examined above. From the slope, a line tension of 0.15 pN is obtained (assuming a viscosity of 10^{-3} Pa/s), which is similar to the value found from static mode analysis (0.12 pN).

We ubiquitously observed line tensions to depend on illumination time, underlining the effect of photooxidation on fluid domain boundary line tension, which has been described before (43). We investigated to what extent illumination intensities influence line tensions and attenuated excitation light intensities by OD filters as indicated in Fig. 7. To determine the dependence of line tension on illumination time, we averaged spectral densities in sequential intervals of 500 consecutive frames and determined line tension values for those time intervals. Fig. 7 indicates that line tensions increase with observation time for all illumination intensities employed and suggests that, for accurate membrane domain line tension measurements, great care must be taken to avoid photoinduced lipid decomposition that by unknown mechanisms increases domain line tensions (43). We note, however, that in addition to photoeffects on line tension, slow domain coarsening could change bulk domain compositions due to thermodynamic equilibration and therefore could contribute to the line tension increase observed in Fig. 7. This aspect will be addressed in future research.

We determined line tension values in 10 vesicles (with composition DOPC/Chol/DPPC = 1:1:1) at the lowest illumination intensity (OD = 1). Analysis of the first 500 frames of the time lapse recording for each vesicle gave a line tension value of 0.064 ± 0.0475 pN from the static trace analysis (Eq. 3) and a value of 0.086 ± 0.0380 pN from the dynamic analysis (Eq. 4). Importantly, a recent contribution found that large (micronscale) domains with boundary line tensions of values determined here are unstable toward breakup into an ensemble of nanoscale hard disks (21). This conclusion was based on a thermodynamic model appropriate for conditions far from the critical point. Accordingly, the domains imaged here are unlikely to result from merger of nanodomains after nucleation. Instead, spinodal decomposition is the likely mechanism of coarsening leading to the domains observed here (6).

DISCUSSION

Fluid domain flicker spectroscopy promises to provide an effective tool for measuring small line tensions in membranes of GUVs and is thus complementary to methods that necessitate line tensions large enough to significantly deform

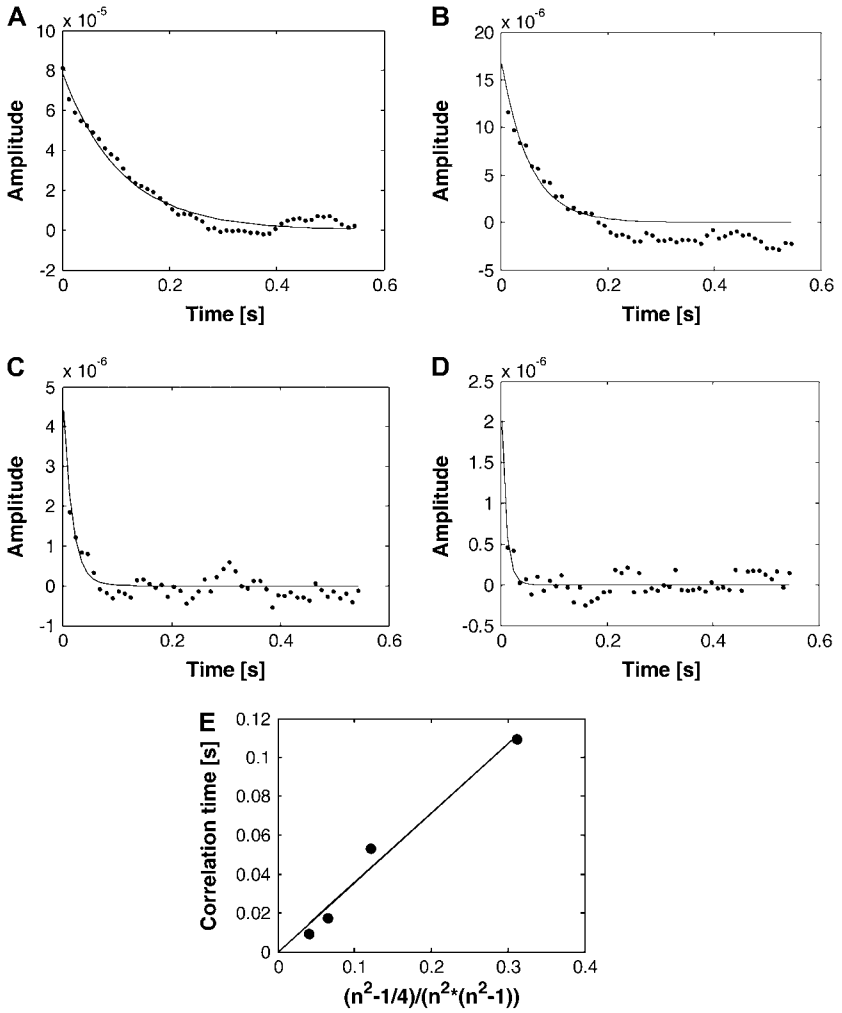

FIGURE 6 (*A–D*) Time autocorrelation functions of modes 2–5: exponential decay is observed. Decay times (correlation times) are obtained from fitting the experimental functions and yield 108, 52, 17, and 9 ms. These relaxation times yield a linear relationship when plotted against a mode number factor given by Eq. 4. The slope of the plot allows determining line tensions alternative to the static fluctuation mode amplitude analysis. A value of 0.15 pN is obtained, which is similar in magnitude compared to the one obtained from analyzing the static mode amplitudes (see Figs. 4 and 5).

vesicle shapes (13,15,24). In contrast to Langmuir monolayer films at the air/water interface, GUVs possess a small membrane area and nonplanar geometry. Techniques that transiently deform domains by application of external forces (such as hydrodynamic flow fields and laser tweezers), which have been successfully used to measure line tensions in domains of Langmuir films (33,34,51), are significantly more difficult to apply to line tension measurements in GUVs. The spectroscopy of thermally excited domain deformations therefore is a valuable alternative. As mentioned above, it is important to be aware of experimental limitations of this technique. In the following, we discuss several effects that have to be considered when trying to accurately measure line tension in GUVs. We first consider limitations imposed by optical imaging of micrometer-sized domains, i.e., pixelization and blurring through the imaging apparatus. These limitations will perturb the experimental Fourier spectrum through aliasing caused by sampling the domain boundary trace with a frequency much below the optimum (Nyquist-) sampling frequency, which is twice the largest fluctuation mode frequency.

We find that simulating fluctuating domain images (see Materials and Methods section) provides an effective tool for investigating systematic deviations from expected line tension values caused by the optical resolution limit, imaging noise, as well as the performance of our tracing algorithm. Domain shapes were calculated through considering 10 fluctuating modes with decreasing mean amplitudes according to Eq. 3. Fig. 8 shows three examples of a fluctuating domain with radius 5 μm, with image pixel size and optical PSF width equivalent to our experimental imaging conditions. Poisson noise was added to the images as detailed in the Materials and Methods section. As Fig. 8 shows, for a domain of radius 5 μm, domain fluctuations at a line tension value of 0.01 pN are easily detected, become more subtle at 0.1 pN, and are almost unnoticeable at 1 pN. For smaller domain radii, the maximum of accurately detectable line tension values becomes smaller. Fig. 9 exemplarily shows results from tracing simulated fluctuating domain images, equivalent to the analysis of experimental domain traces. Fig. 9 *A* indicates that a domain of 5 μm radius and 0.1 pN line tension allows determining line tension from static mode amplitude analysis at least up to the 10th mode.

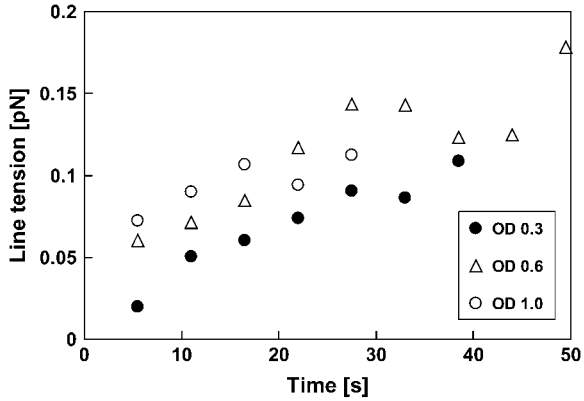

FIGURE 7 Line tensions measured in single domains of three different vesicles as a function of observation time and illumination intensity obtained from static trace analysis. Vesicles were illuminated continuously, and 500 frames were analyzed per time interval to obtain an averaged line tension for that interval. OD values indicate attenuation of excitation light relative to the maximum intensity (which was not measured) by means of neutral density filters. Line tension is observed to increase significantly during illumination intervals for all excitation intensities.

Conversely, FFT analysis of domain traces with the same value of R_0, but the higher line tension of 1 pN shows significant deviation of line tension values in the first mode ($n = 2$), and deviations increase with higher mode numbers. This deviation from capillary wave theory expectation is further demonstrated in the plot shown in Fig. 9 *C*. To minimize inaccurate determination of boundary fluctuations caused by imaging a planar slice of a spherical surface, domains used for boundary flicker spectroscopy should be small relative to the vesicle size. Fig. 9, *D* and *E*, shows that in domains of 2.5 μm radius and line tension of 0.1 pN, the first four modes contain relatively accurate line tension information. Again, line tensions of 1 pN cannot be measured (data not shown). Fig. 9, *F* and *G*, shows line tension analysis results from tracing a domain of radius 10 μm and line tension of 1 pN. The first four modes are observed to follow capillary wave theory. Domains of this size, however, are expected to cause tracing error due to the orthogonal projection involved in imaging a spherical vesicle of sizes typically not significantly larger than this domain size (57). Further inaccuracies for large domain size are introduced by focusing errors due to the finite microscopy objective depth of field. Furthermore, for large line tensions, CCD camera integration time has to be considered when evaluating domain boundary fluctuations (see below and Fig. 10). However, for line tensions above ~0.5 pN, alternative approaches for measuring line tensions in GUVs are available (22,25).

Besides limitations caused by the optical imaging system, the camera exposure time with which fluctuating domains are imaged has to be considered. Finite CCD camera frame acquisition times will lead to averaging over fast fluctuation modes. This effect has been investigated in detail in the analysis of three-dimensional GUV shape fluctuations (52,54,68). From a time average of the angular autocorrelation function over a time interval given by the frame acquisition time, a factor can be derived that quantitatively describes the deviations of experimentally measured mode powers $|u_n|^{2*}$ from the real amplitudes $|u_n|^2$. This factor depends on the ratio of mode relaxation time τ_n and camera integration time τ_s:

$$|u_n|^{2*} = 2\left(\frac{\tau_n}{\tau_s}\right)^2\left[\frac{\tau_s}{\tau_n} + \exp\left(-\frac{\tau_s}{\tau_n}\right) - 1\right]|u_n|^2. \qquad (5)$$

This factor is equal to 1 for infinitely short camera frame acquisition times, as can be seen from expanding the exponential term to second order. If long camera acquisition times cannot be avoided, then by means of Eq. 5 modes with correlation times that approach the camera acquisition time can in principle be corrected in an iterative procedure (52) that, however, is dependent on the model (here Eq. 4) used to determine theoretical values for mode relaxation times.

CONCLUSIONS

We have applied domain boundary flicker spectroscopy to examine line tension in domains of vesicles with a single composition. This method should allow accurate determination of fluid domain boundary line tension composition and temperature (23) dependence in regimes where small line tensions (below 1 pN) are observed. Experimental conditions have to be accounted for that limit the accessible line tension and fluctuation mode range. Sources for these limitations

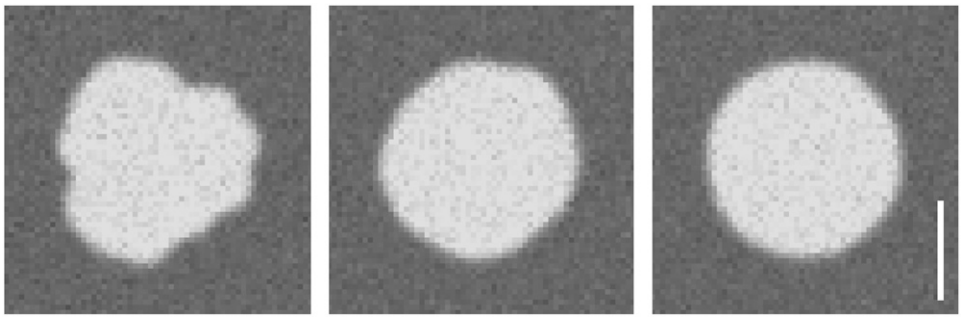

FIGURE 8 Computationally obtained fluctuating domains with line tension of 0.01, 0.1, and 1 pN, radius $R_0 = 5$ μm, and imaging conditions (pixel size, optical PSF width) equivalent to experimental conditions. For each domain, 10 fluctuation modes were considered (see Materials and Methods section). Additionally, Poisson noise was added to the domain images, where the pixel intensities were modulated via a Poisson noise generator assuming a variance as given by the undistorted pixel intensity.

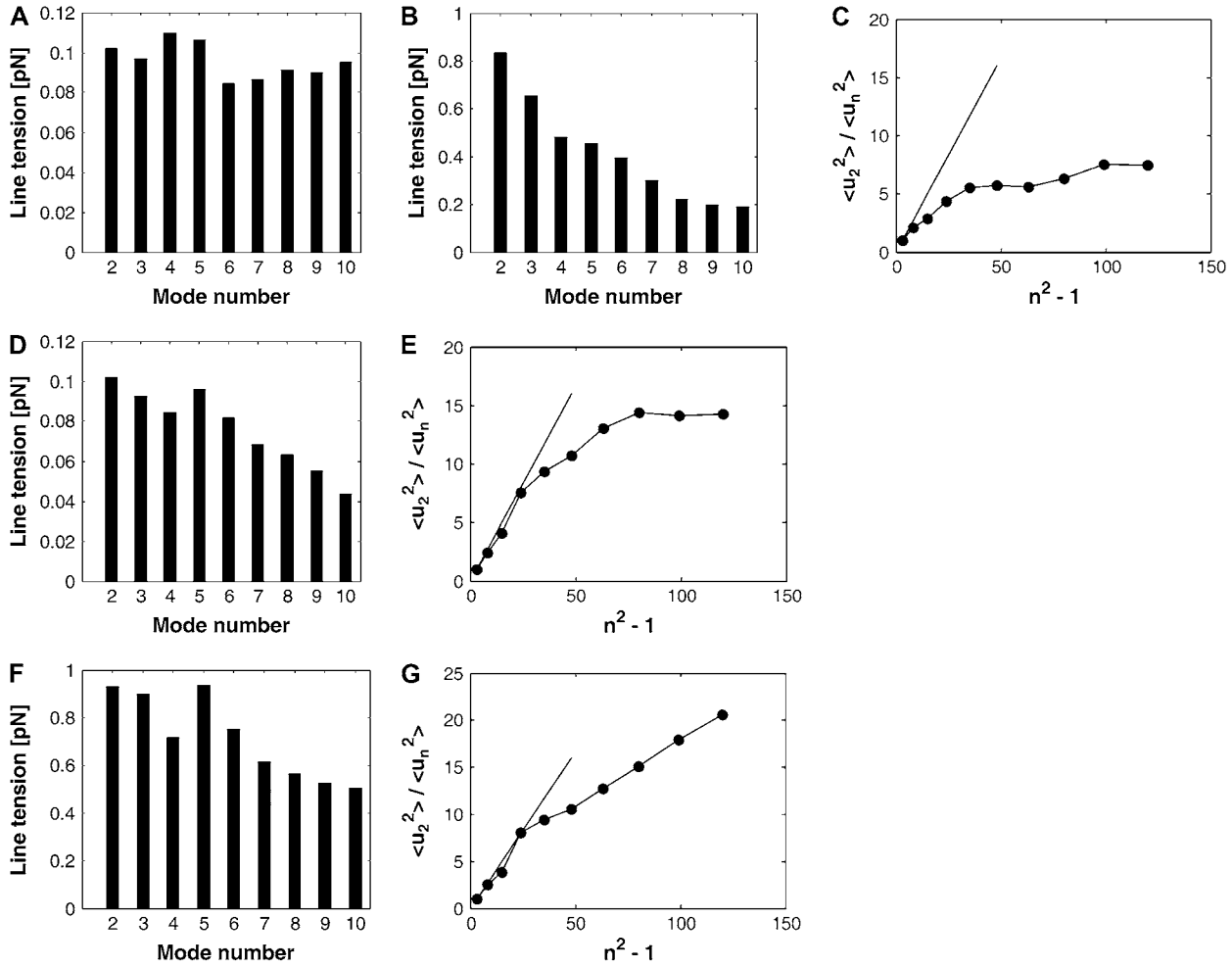

FIGURE 9 Simulated domains traced and analyzed equivalently to experimental shapes. Mean values of line tensions and spectral densities are obtained from averaging trace results from 200 simulated domain shapes, generated from random numbers according to the Materials and Methods section. (*First row*) domain radius 5μm. (*A*) Line tension 0.1 pN. (*B* and *C*) Line tension 1 pN. For this domain size, the smaller line tension can be accurately determined, whereas a line tension of 1 pN is not accurately returned by tracing and FFT analysis. (*Second row*) domain radius 2.5 μm, line tension 0.1 pN. For this domain size and line tension, the first four modes yield accurate line tension information. (*Third row*) domain radius 10 μm, line tension 1 pN.

include the pixel size and resolution of the optical imaging system, fluorescence camera frame acquisition rates, fluorescence illumination intensity, and domain/vesicle size ratio.

We suggest that the method examined here can contribute to the identification of potential ''line active'' components, i.e., membrane-associated molecules that modulate line tension by differential partitioning between boundary interface region and domain bulk region. Since such molecules could stabilize two-dimensional lipid membrane microemulsions (69), they could be of significance for understanding physical chemical aspects of the putative biological ''membrane rafts''.

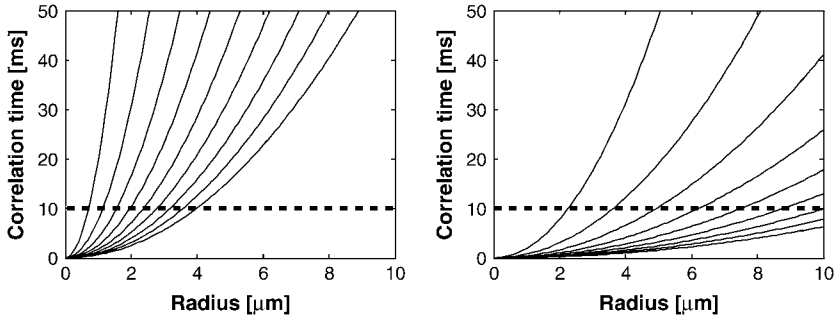

FIGURE 10 Correlation (relaxation) times for mode numbers 2 (*leftmost* plot in both graphs) to 10 (*rightmost* plot in both graphs) as a function of domain radius, obtained from Eq. 4, assuming a viscosity of 10^{-3} Pa/s, and a line tension of 0.1 pN (*left*) and 1 pN (*right*). As follows from Eq. 4, correlation times decrease with increasing line tension, an effect which has to be considered when imaging fluctuating domains with large line tension and nonzero camera frame acquisition time. For accurate experimental determination of mode powers, the relaxation time should not be smaller compared to the camera frame acquisition time (10 ms in our experiments, see *dashed lines*).

APPENDIX: DERIVATION OF EQS. 1 AND 2

A. Domain area. To obtain the expression for the domain area, Eq. 2, we assume a Fourier expansion of the static contour profile according to

$$r(\theta) = R_0\left(1 + u_0 + \sum_{n>0} a_n \cos n\theta + \sum_{n>0} b_n \sin n\theta\right) = R_0\left(1 + u_0 + \frac{1}{2}\sum_{n\neq 0} u_n \exp(in\theta)\right), \quad (6)$$

where a_n and b_n are real numbers, u_n are complex numbers, and $|u_n|^2 = a_n^2 + b_n^2$, because $u_n = a_n \pm ib_n$, for $n < 0$ (upper) and $n > 0$ (lower). The coefficients a_n and b_n are related to mode amplitude $|u_n|$ and phase shift δ_n, relative to a reference point on the boundary trace by $a_n = |u_n|\cos\delta_n$ and $b_n = |u_n|\sin\delta_n$. The domain area is obtained from integration: $A = (1/2)\int_0^{2\pi} r(\theta)^2 d\theta$ to yield

$$A = \frac{R_0^2}{2}\int_0^{2\pi}\left(1 + u_0 + \frac{1}{2}\sum_{n<0} u_n \exp(in\theta) + \frac{1}{2}\sum_{n>0} u_n \exp(in\theta)\right)\left(1 + u_0 + \frac{1}{2}\sum_{n'<0} u_n \exp(in\theta) + \frac{1}{2}\sum_{n'>0} u_n \exp(in\theta)\right)d\theta,$$

from which we obtain $A = (R_0^2/2)(\sum_{n<0}(u_n\bar{u}_n/4) + (1+u_0)^2 + \sum_{n>0}(u_n\bar{u}_n/4))2\pi = \pi R_0^2((1+u_0)^2 + (1/2)\sum_{n>0}|u_n|^2)$, where a bar indicates a complex conjugate. We can eliminate u_0 in the expression of $r(\theta)$ (Eq. 6) with $u_0 \approx -(1/4)\sum_n |u_n|^2$ to obtain for the angular average of the domain radius $\langle r(\theta)\rangle = R_0(1 - (1/4)\sum_n \langle |u_n|^2\rangle)$. It is observed that $\langle r(\theta)\rangle$ is smaller than R_0 for fluctuating domains, which is a consequence of area conservation.

B. Contour length. To derive the expression for the contour length L (Eq. 2), we need the angular derivative of the radius vector $\vec{r}$, to obtain $L = \int_0^{2\pi} |\dot{\vec{r}}| d\theta$, where $|\dot{\vec{r}}| = \sqrt{r^2 + \dot{r}^2}$, and a dot indicates derivative with respect to θ. From Eq. 6, it is found that

$$|\dot{\vec{r}}| = R_0\left\{\left(1 + u_0 + \frac{1}{2}\sum_n u_n \exp(in\theta)\right)^2 + \left(\frac{1}{2}\sum_n inu_n \exp(in\theta)\right)^2\right\}^{1/2}$$
$$= R_0(1+u_0)\left\{1 + \frac{1}{1+u_0}\sum_n u_n \exp(in\theta) + \frac{1}{4(1+u_0)^2}\left[\left(\sum_n u_n \exp(in\theta)\right)^2 - \left(\sum_n u_n\, n \exp(in\theta)\right)^2\right]\right\}^{1/2}$$
$$= R_0(1+u_0)\left\{1 + \frac{1}{2(1+u_0)}\sum_n u_n \exp(in\theta) - \frac{1}{8(1+u_0)^2}\left(\sum_n u_n \exp(in\theta)\right)^2 + \frac{1}{8(1+u_0)^2}\left[\left(\sum_n u_n \exp(in\theta)\right)^2 - \left(\sum_n u_n\, n \exp(in\theta)\right)^2\right]\right\}$$

where the last line is obtained from expanding the square root to second order. Integration over the angle results in $L = 2\pi R_0\{1 + u_0 + (1/4(1+u_0))\sum_{n>0} u_n\bar{u}_n n^2\}$, from which we obtain Eq. 2, after inserting for $1+u_0$ into (and Taylor expansion of) the last term.

We are indebted to Gerhard Gompper, who introduced us to capillary wave theory, and we acknowledge discussions with Sovan Das and Aurelia Honerkamp-Smith.

C.E. acknowledges a fellowship from the European Social Fund—National Operative Program 2000–2006. This work was supported in part by the National Science Foundation sponsored UPenn Materials Research Science and Engineering Center, Award No: DMR05-20020.

REFERENCES

1. Dietrich, C., L. A. Bagatolli, Z. N. Volovyk, N. L. Thompson, M. Levi, K. Jacobson, and E. Gratton. 2001. Lipid rafts reconstituted in model membranes. *Biophys. J.* 80:1417–1428.
2. Samsonov, A. V., I. Mihalyov, and F. S. Cohen. 2001. Characterization of cholesterol-sphingomyelin domains and their dynamics in bilayer membranes. *Biophys. J.* 81:1486–1500.
3. Ipsen, J. H., G. Karlstroem, O. G. Mouritsen, H. Wennerstroem, and M. J. Zuckermann. 1987. Phase equilibria in the phosphatidylcholine-cholesterol system. *Biochim. Biophys. Acta.* 905:162–172.
4. Veatch, S. L., and S. L. Keller. 2005. Seeing spots: complex phase behavior in simple membranes. *Biochim. Biophys. Acta.* 1746:172–185.
5. Veatch, S. L., and S. L. Keller. 2002. Organization in lipid membranes containing cholesterol. *Phys. Rev. Lett.* 89:268101.
6. Veatch, S. L., and S. L. Keller. 2003. Separation of liquid phases in giant vesicles of ternary mixtures of phospholipids and cholesterol. *Biophys. J.* 85:3074–3083.
7. Veatch, S. L., I. V. Polozov, K. Gawrisch, and S. L. Keller. 2004. Liquid domains in vesicles investigated by NMR and fluorescence microscopy. *Biophys. J.* 86:2910–2922.
8. Veatch, S. L., and S. L. Keller. 2005. Miscibility phase diagrams of giant vesicles containing sphingomyelin. *Phys. Rev. Lett.* 94:148101.
9. Veatch, S. L., K. Gawrisch, and S. L. Keller. 2006. Closed-loop miscibility gap and quantitative tie-lines in ternary membranes containing diphytanoyl PC. *Biophys. J.* 90:4428–4436.
10. Kahya, N., D. Scherfeld, K. Bacia, B. Poolman, and P. Schwille. 2003. Probing lipid mobility of raft-exhibiting model membranes by fluorescence correlation spectroscopy. *J. Biol. Chem.* 278:28109–28115.
11. Scherfeld, D., N. Kahya, and P. Schwille. 2003. Lipid dynamics and domain formation in model membranes composed of ternary mixtures of unsaturated and saturated phosphatidylcholines and cholesterol. *Biophys. J.* 85:3758–3768.
12. Cicuta, P., S. L. Keller, and S. L. Veatch. 2007. Diffusion of liquid domains in lipid bilayer membranes. *J. Phys. Chem. B.* 111:3328–3331.
13. Baumgart, T., S. T. Hess, and W. W. Webb. 2003. Imaging coexisting fluid domains in biomembrane models coupling curvature and line tension. *Nature.* 425:821–824.
14. Bacia, K., P. Schwille, and T. Kurzchalia. 2005. Sterol structure determines the separation of phases and the curvature of the liquid-ordered phase in model membranes. *Proc. Natl. Acad. Sci. USA.* 102:3272–3277.

15. Baumgart, T., S. Das, W. W. Webb, and J. T. Jenkins. 2005. Membrane elasticity in giant vesicles with fluid phase coexistence. *Biophys. J.* 89: 1067–1080.

16. Edidin, M. 2003. The state of lipid rafts: from model membranes to cells. *Annu. Rev. Biophys. Biomol. Struct.* 32:257–283.

17. Munro, S. 2003. Lipid rafts: elusive or illusive? *Cell.* 115:377–388.

18. Akimov, S. A., P. I. Kuzmin, J. Zimmerberg, F. S. Cohen, and Y. A. Chizmadzhev. 2004. An elastic theory for line tension at a boundary separating two lipid monolayer regions of different thickness. *J. Electroanal. Chem.* 564:13–18.

19. Kuzmin, P. I., S. A. Akimov, Y. A. Chizmadzhev, J. Zimmerberg, and F. S. Cohen. 2005. Line tension and interaction energies of membrane rafts calculated from lipid splay and tilt. *Biophys. J.* 88:1120–1133.

20. Akimov, S. A., P. I. Kuzmin, J. Zimmerberg, and F. S. Cohen. 2007. Lateral tension increases the line tension between two domains in a lipid bilayer membrane. *Phys. Rev. E Stat. Nonlin. Soft Matter Phys.* 75:011919.

21. Frolov, V. A. J., Y. A. Chizmadzhev, F. S. Cohen, and J. Zimmerberg. 2006. ''Entropic traps'' in the kinetics of phase separation in multi-component membranes stabilize nanodomains. *Biophys. J.* 91:189–205.

22. Tian, A., C. Johnson, W. Wang, and T. Baumgart. 2007. Line tension at fluid membrane domain boundaries measured by micropipette aspiration. *Phys. Rev. Lett.* 98:208102.

23. Honerkamp-Smith, A. R., P. Cicuta, and S. L. Keller. 2007. Critical fluctuations in a lipid bilayer with two liquid phases. *Biophys. J.* 92: 61a. (Abstr.)

24. Idema, T., S. Semrau, and C. Storm. 2007. Towards understanding the shape of multi-component bilayer vesicles. *Biophys. J.* 92:583a. (Abstr.)

25. Blanchette, C. D., W. C. Lin, C. A. Orme, T. V. Ratto, and M. L. Longo. 2007. Using nucleation rates to determine the interfacial line tension of symmetric and asymmetric lipid bilayer domains. *Langmuir.* 23:5875–5877.

26. Gibbs, J. W. 1878. On the equilibrium of heterogeneous substances. *Transactions of the Connecticut Academy.* 3:343–524.

27. Rowlinson, J. S., and B. Widom. 1982. Three-phase equilibrium. *In* Molecular Theory of Capillarity. Oxford University Press, New York.

28. Perkovic, S., E. M. Blokhuis, E. Tessler, and B. Widom. 1995. Boundary tension: from wetting transition to prewetting critical point. *J. Chem. Phys.* 102:7584–7595.

29. Mann, E. K., S. Henon, D. Langevin, and J. Meunier. 1992. Molecular layers of a polymer at the free-water surface—microscopy at the Brewster-angle. *J. Phys. II.* 2:1683–1704.

30. Roberts, M. J., E. J. Teer, and R. S. Duran. 1997. Measurement of line tension from cell coalescence events in a Langmuir film. *J. Phys. Chem. B.* 101:699–701.

31. Muller, P., and F. Gallet. 1991. First measurement of the liquid-solid line energy in a Langmuir monolayer. *Phys. Rev. Lett.* 67:1106–1109.

32. Stine, K. J., C. M. Knobler, and R. C. Desai. 1990. Buckling instability in monolayer network structures. *Phys. Rev. Lett.* 65:1004–1007.

33. Benvegnu, D. J., and H. M. McConnell. 1992. Line tension between liquid domains in lipid monolayers. *J. Phys. Chem.* 96:6820–6824.

34. Wurlitzer, S., P. Steffen, and T. M. Fischer. 2000. Line tension of Langmuir monolayer phase boundaries determined with optical tweezers. *J. Chem. Phys.* 112:5915–5918.

35. Goldstein, R. E., and D. P. Jackson. 1994. Domain shape relaxation and the spectrum of thermal fluctuations in Langmuir monolayers. *J. Phys. Chem.* 98:9626–9636.

36. Hu, Y. F., K. Meleson, and J. Israelachvili. 2006. Thermodynamic equilibrium of domains in a two-component Langmuir monolayer. *Biophys. J.* 91:444–453.

37. Zhelev, D. V., and D. Needham. 1993. Tension-stabilized pores in giant vesicles—determination of pore-size and pore line tension. *Biochim. Biophys. Acta.* 1147:89–104.

38. Puech, P. H., N. Borghi, E. Karatekin, and F. Brochard-Wyart. 2003. Line thermodynamics: adsorption at a membrane edge. *Phys. Rev. Lett.* 90:128304.

39. Karatekin, E., O. Sandre, H. Guitouni, N. Borghi, P. H. Puech, and F. Brochard-Wyart. 2003. Cascades of transient pores in giant vesicles: line tension and transport. *Biophys. J.* 84:1734–1749.

40. de Joannis, J., F. Y. Jiang, and J. T. Kindt. 2006. Coarse-grained model simulations of mixed-lipid systems: composition and line tension of a stabilized bilayer edge. *Langmuir.* 22:998–1005.

41. Seul, M., and M. J. Sammon. 1990. Competing interactions and domain-shape instabilities in a monomolecular film at an air-water interface. *Phys. Rev. Lett.* 64:1903–1906.

42. Stone, H. A., and H. M. Mcconnell. 1995. Hydrodynamics of quantized shape transitions of lipid domains. *Proc. Royal Society of London Series A-Mathematical and Physical Sciences.* 448:97–111.

43. Ayuyan, A. G., and F. S. Cohen. 2006. Lipid peroxides promote large rafts: effects of excitation of probes in fluorescence microscopy and electrochemical reactions during vesicle formation. *Biophys. J.* 91: 2172–2183.

44. Milner, S. T., and S. A. Safran. 1987. Dynamical fluctuations of droplet emulsions and vesicles. *Phys. Rev. A.* 36:4371–4379.

45. Safran, S. A. 1983. Fluctuations of spherical microemulsions. *J. Chem. Phys.* 78:2073–2076.

46. Henderson, J. R., and P. Schofield. 1982. Statistical-mechanics of a fluid drop. *Proc. Royal Society of London Series A-Mathematical Physical and Engineering Sciences.* 380:211–227.

47. Schneider, M. B., J. T. Jenkins, and W. W. Webb. 1984. Thermal fluctuations of large quasi-spherical bimolecular phospholipid vesicles. *J. Phys. [E].* 45:1457–1472.

48. Sackmann, E., H. P. Duwe, and H. Engelhardt. 1986. Membrane bending elasticity and its role for shape fluctuations and shape transformations of cells and vesicles. *Faraday Discuss.* 81:281–290.

49. Duwe, H. P., and E. Sackmann. 1990. Bending elasticity and thermal excitations of lipid bilayer vesicles: modulation by solutes. *Physica A.* 163:410–428.

50. Engelhardt, H., H. P. Duwe, and E. Sackmann. 1985. Bilayer bending elasticity measured by Fourier-analysis of thermally excited surface undulations of flaccid vesicles. *J. Phys. Lett.* 46:L395–L400.

51. Mann, E. K., S. Henon, D. Langevin, J. Meunier, and L. Leger. 1995. Hydrodynamics of domain relaxation in a polymer monolayer. *Phys. Rev. E.* 51:5708–5720.

52. Faucon, J. F., M. D. Mitov, P. Meleard, I. Bivas, and P. Bothorel. 1989. Bending elasticity and thermal fluctuations of lipid membranes. Theoretical and experimental requirements. *J. Phys.* 50:2389–2414.

53. Henriksen, J., A. C. Rowat, and J. H. Ipsen. 2004. Vesicle fluctuation analysis of the effects of sterols on membrane bending rigidity. *Eur. Biophys. J.* 33:732–741.

54. Pecreaux, J., H. G. Dobereiner, J. Prost, J. F. Joanny, and P. Bassereau. 2004. Refined contour analysis of giant unilamellar vesicles. *Eur. Phys. J. E.* 13:277–290.

55. Gelfand, M. P., and M. E. Fisher. 1990. Finite-size effects in fluid interfaces. *Physica A.* 166:1–74.

56. Safran, S. A. 2003. Statistical Thermodynamics of Surfaces, Interfaces, and Membranes. Westview Press, Boulder, CO.

57. Mathivet, L., S. Cribier, and P. F. Devaux. 1996. Shape change and physical properties of giant phospholipid vesicles prepared in the presence of an AC electric field. *Biophys. J.* 70:1112–1121.

58. Veatch, S. L., and S. L. Keller. 2003. A closer look at the canonical 'raft mixture' in model membrane studies. *Biophys. J.* 84:725–726.

59. Roux, A., D. Cuvelier, P. Nassoy, J. Prost, P. Bassereau, and B. Goud. 2005. Role of curvature and phase transition in lipid sorting and fission of membrane tubules. *EMBO J.* 24:1537–1545.

60. Press, W. H., B. P. Flannery, S. A. Teukolsky, and W. T. Vetterling. 1989. Numerical Recipes. Cambridge University Press, New York.

61. Seul, M., M. J. Sammon, and L. R. Monar. 1991. Imaging of fluctuating domain shapes—methods of image-analysis and their implementation in a personal computing environment. *Rev. Sci. Instrum.* 62:784–792.

62. Doebereiner, H. G., E. Evans, M. Kraus, U. Seifert, and M. Wortis. 1997. Mapping vesicle shapes into the phase diagram: a comparison of experiment and theory. *Physical Review E.* 55:4458–4473.

63. Chandler, D. 1987. Introduction to Modern Statistical Mechanics. Oxford University Press, New York.

64. Bivas, I., P. Hanusse, P. Bothorel, J. Lalanne, and O. Aguerrechariol. 1987. An application of the optical microscopy to the determination of the curvature elastic-modulus of biological and model membranes. *J. Phys. [E].* 48:855–867.

65. Seul, M. 1993. Dynamics of domain shape relaxation in Langmuir films. *J. Phys. Chem.* 97:2941–2945.

66. Alexander, J. C., A. J. Bernoff, E. K. Mann, J. A. Mann, J. R. Wintersmith, and L. Zou. 2007. Domain relaxation in Langmuir films. *J. Fluid Mech.* 571:191–219.

67. Saffman, P. G., and M. Delbruck. 1975. Brownian-motion in biological-membranes. *Proc. Natl. Acad. Sci. USA.* 72:3111–3113.

68. Meleard, P., J. F. Faucon, M. D. Mitov, and P. Bothorel. 1992. Pulsed-light microscopy applied to the measurement of the bending elasticity of giant liposomes. *Europhys. Lett.* 19:267–271.

69. Simons, K., and W. L. C. Vaz. 2004. Model systems, lipid rafts, and cell membranes. *Annu. Rev. Biophys. Biomol. Struct.* 33:269–295.